A Fresh Look at Jovian Decametric Radio Emission Occurrence Probabilities in the CML-Io Phase Plane

David Typinski[1], Charles Higgins[2], Richard Flagg[3], Wes Greenman[4], Jim Sky[5], Roger Giuntini[6], Francisco Reyes[7], Shing Fung[8], James Brown[9], Thomas Ashcraft[10], Larry Dodd[11], James Thieman[12], and Leonard Garcia[13]

[1]AJ4CO Observatory, High Spring, FL 32655, [2]Dept. of Physics & Astronomy, Middle Tennessee State University, Murfreesboro, TN 37132, [3]RF Associates, Honolulu, HI 96826, [4]LGM Radio Alachua, Alachua, FL 32615, [5]Radio Sky Publishing, Louisville, KY, 40214, [6]Dept. of Physics & Astronomy, Middle Tennessee State University, Murfreesboro, TN 37132, [7]Department of Astronomy, University of Florida, Gainesville, FL 32611, [8]ITMPL/NASA GSFC, Greenbelt MD 20771, [9]Hawks Nest Radio Astronomy Observatory, Industry, PA 15052, [10]Heliotown Observatory, Lamy, NM 87540, [11]Georgia Amateur Radio Astronomy Observatory, Jasper, GA 30143, [12]UMBC/NASA GSFC, Greenbelt MD 20771, [13]SGT/NASA GSFC, Greenbelt MD 20771

Introduction

The occurrence of Jovian decametric emission (DAM) is sporadic as observed from ground-based instruments. When the timing intervals of observed occurrences of Jovian DAM are compared to all periods when Jupiter was observable, a set of Jovian DAM emission occurrence probabilities can be created. These probabilities are usefully plotted as a function of Jovian system III (magnetospheric) central meridian longitude (CML-III) and Io's phase measured from superior geocentric conjunction (SGC), producing a CML-Io phase plane. Bigg showed in 1964 that Jovian DAM tends to have higher occurrence probabilities in different regions of the CML-Io phase plane, leading to the identification of different Io-related and non-Io-related DAM components. These probabilities assist determination of the rotation rate of Jupiter's core and aid the development of theories about how and why Jovian DAM is radiated.

Instrumentation

AJ4CO Observatory, located in High Springs, Florida, USA, has been observing Jupiter when its elevation is ≥ 10° since October, 2013. The primary instrument used for observing Jovian DAM is a swept-frequency (16 to 32 MHz) dual polarization spectrograph fed by an eight-element phased array of terminated folded dipoles. A high-speed digital spectrograph with a tunable 2 MHz bandwidth was also used from 2013 to 2016 to observe emission at higher time resolution.

Dynamic Spectra

We analyzed the dynamic spectra of Jovian DAM observed at AJ4CO Observatory from 2013 through 2020 to measure emission timing intervals and classify the emission into four types: L (for wideband L bursts), S (for wideband S bursts), N (for narrowband continuous emission), and T (for narrowband trains of S bursts). We also classified each emission event by dominant polarization and emission envelope arc shape or frequency drift direction.

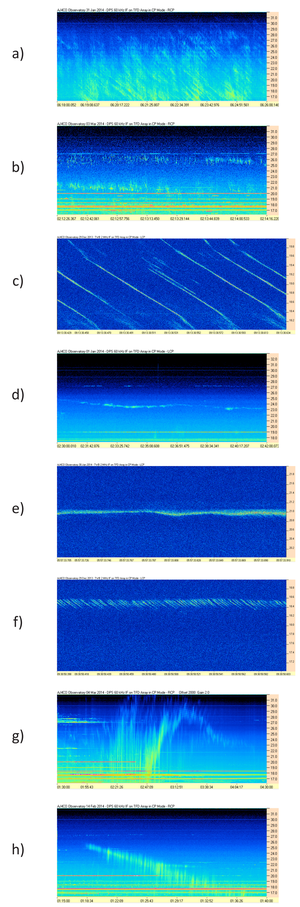

Figure 1 – Example dynamic spectra of different types of Jovian DAM. Time UTC on horizontal axis; radio frequency in MHz on vertical axis; amplitude represented by color. a) L bursts, b) S bursts (150 ms resolution), c) S bursts (205 µs resolution), d) N event (150 ms resolution), e) N event (205 µs resolution), f) Narrow band S burst train (205 µs resolution), g) vertex early arcs, h) downward frequency drift emission envelope.

Phase Plane Representation of Planetary Geometry

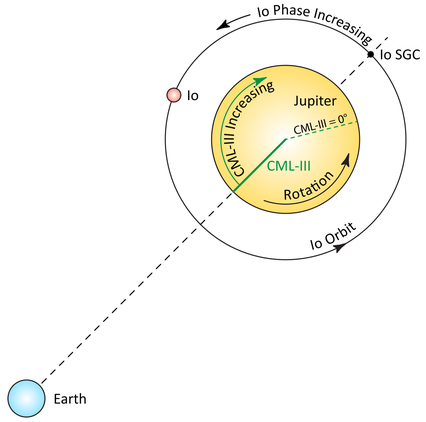

Figure 2 – Geometric relationship between Earth, Io, Jupiter, and Io phase relative to superior geocentric conjunction (Io SGC). Io phase increases as Io orbits past SGC where Io phase = 0°. Jupiter's System III central meridian longitude (CML-III) is Earth's Jovian longitude with respect to the Jovian magnetic field. CML-III increases as Jupiter rotates. CML-III = 0° (i.e., the Jovian magnetosphere's prime meridian) does not correspond with any particular feature of the magnetic field (Seidelmann, 1977; Archinal, 2011). **Jovian DAM is observed much more often for several unique combinations of CML-III and Io Phase.** For any observation of Jovian DAM, the emission event can be plotted against CML-III and Io phase to generate a track as shown in Figure 3.

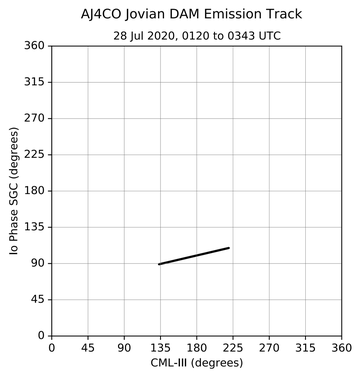

Figure 3 – An instance of observed Jovian DAM plotted on the CML-Io phase plane. This plane is a mathematical construct. It does not represent any physical feature of Jupiter or the Jovian magnetic field. The track plotted represents the duration over which Jovian DAM was observed.

Methodology

We observed the radio spectrum from 16 to 32 MHz for seven years (26 Sep 2013 to 26 Sep 2020) with an observatory uptime of 98%. Each 24-hour dynamic spectrum was analyzed for presence of Jovian DAM during the period when Jupiter's elevation was ≥ 10°. All observed Jovian DAM emission event dynamic spectra were then analyzed for timing every two MHz over the observed frequency range. Each emission event at each frequency analyzed was logged with the associated telescope and emission parameters. Emission parameters included radio frequency, start and stop times, polarization, burst type, and envelope arc shape or frequency drift direction. The log entries were then processed to add ephemerides from JPL Horizons including CML-III and Io phase (Giorgini).

Phase plane tracks (ref. Fig. 3) from all observed emission events (Jovian DAM "occurrences") were then summed in 5° by 5° bins to produce a 72 by 72 element matrix of emission occurrence counts.

Similarly, phase plane tracks representing the times when Jupiter was being observed (Jupiter "watches," the times when the observatory was operational and Jupiter was above 10° elevation) – regardless of whether any Jovian DAM emission was observed – were also summed and binned.

The emission event occurrence bins matrix was then divided by the watch bins matrix in element-by-element fashion (Hadamard division) to produce a matrix of CML-Io phase plane of emission probabilities which was then plotted as shown in Figure 4.

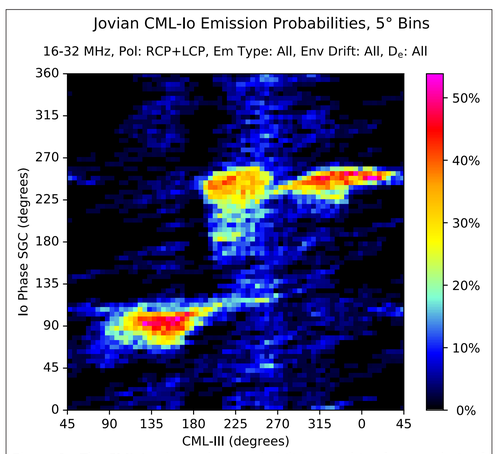

Figure 4 – The CML-Io phase plane probabilities resulting from analysis of all emission events present in seven years of AJ4CO data. Note that the horizontal axis has been shifted by 45° to minimize the amount of high-probability area crossing the plot boundaries.

The probabilities of each polarization are markedly different. We found it useful to separate the probabilities by polarization, as shown in Figure 5, in all further analysis.

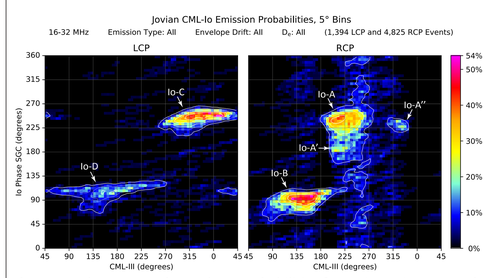

Figure 5 – The CML-Io phase plane probabilities from Figure 3 separated into left circular and right circular polarizations (LCP and RCP). Maximum probability for LCP and RCP is 54%. In this plot, solid contours represent odd integral multiples of probability standard deviation (σ) and dashed contours represent even multiples. σ_{LCP} = 4.8% and σ_{RCP} = 6.7%, equivalent to 8.9% and 12% of maximum probability respectively.

Analysis of Figure 5 determines the 1σ probability extents on the CML-Io phase plane as outlined in Table 1. **We note that the Io-D zone extends 30° lower in Io Phase than previously reported** (Carr, 1983; Garcia, 1996; Marques, 2017).

Phase Plane Zone	CML Range (°)	Io Phase Range (°)
Io-A	180 – 280	160 – 265
Io-A′	195 – 255	160 – 195
Io-A′′	305 – 335	215 – 245
Io-B	70 – 210	50 – 120
Io-B′	100 – 175 *	65 – 95 *
Io-C	255 – 55	210 – 265
Io-D	5 – 270	65 – 125

Table 1 – Extents of the Io controlled emission 1σ probability zones on the CML Io phase plane. The division between Io-A and Io-A′ does not decrease below 1σ, but is plainly visible at Io phase 195°. *The Io-B′ zone appears not as a difference in emission probability, but as a difference in emission type. Here we use the 2σ contour (to account for reduced maximum probability) shown in the RCP narrow band phase plane in Figure 7.

We analyzed subsets of the data to produce probability phase plane plots by frequency, emission type, and envelope drift direction. While the number of permutations is too large to permit reproduction here, a sample of the plots with the most interesting results are shown.

Analysis of Figure 6 determines the extents of the non-Io-controlled emission (occurrence limits only) as outlined in Table 2.

Phase Plane Zone	CML Range (°)
non-Io-A	200 – 350
non-Io-A′	290 – 350
non-Io-B	55 – 275
non-Io-C	210 – 40
non-Io-D	70 – 20

Table 2 – Extents of the occurrence of non-Io-controlled emission.

Figure 6 shows how the phase plane probabilities change with frequency drift or arc shape. The combination of polarization and emission arc shape or drift direction are unique to each phase plane zone and can serve to define the zones as in Table 3.

Phase Plane Zone	Polarization	Arc Shape / Envelope Freq. Drift
Io-A / A′ / A″	RCP	Vertex Late / Downward
Io-B / B′	RCP	Vertex Early / Upward
Io-C	LCP	Vertex Late / Downward
Io-D	LCP	Vertex Early / Upward

Table 3 – Phase plane high probability zone emission characteristics.

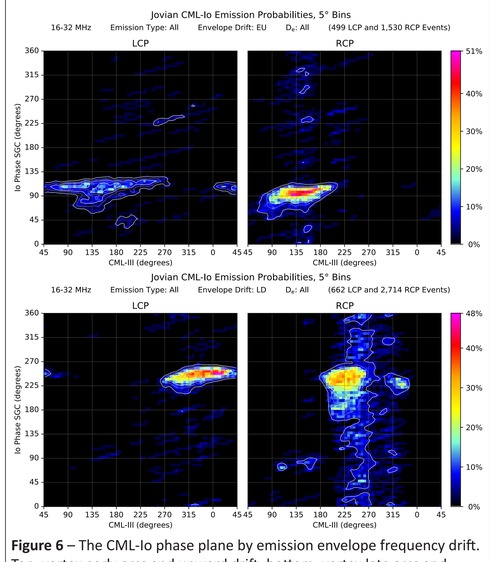

Figure 6 – The CML-Io phase plane by emission envelope frequency drift. Top, vertex early arcs and upward drift; bottom, vertex late arcs and downward drift.

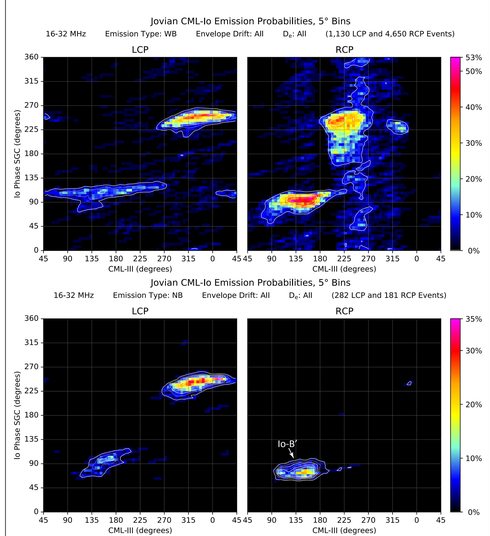

Figure 7 – The CML-Io phase plane by emission bandwidth. Top, wideband emission (L and S bursting); bottom, narrow band emission (N events and narrow band trains of S bursts). The Io-B′ zone (RCP narrow band) is clearly differentiated from Io-B (RCP wideband).

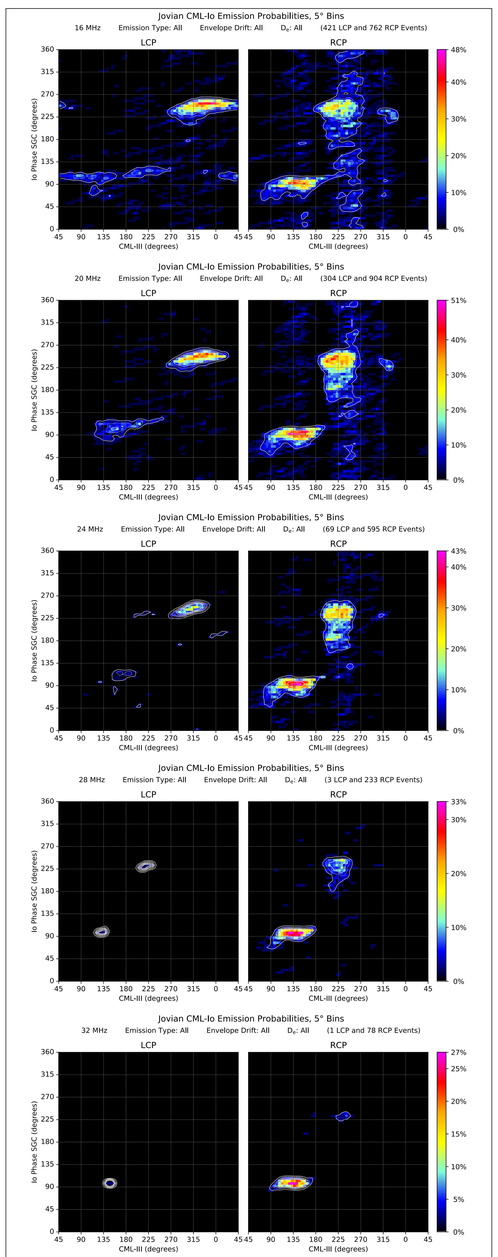

Figure 8 – The CML-Io phase plane by emission radio frequency. The high probability regions decrease in area as radio frequency increases because Jovian DAM in the frequncy range being studied (16 to 32 MHz) becomes weaker and occurs less frequently as radio frequency increases.

Conclusion

Analysis of seven years of Jovian DAM dynamic spectral data recorded by AJ4CO Observatory produces CML-Io phase plane probabilities in good agreement with published values with one exception: we find the Io-D zone extends 30° lower in Io phase than previously reported.

References

Archinal, B. A., et al. (2011). Report of the IAU Working Group on Cartographic Coordinates and Rotational Elements: 2009. *Celestial Mechanics and Dynamical Astronomy*, 109, 111-135. https://doi.org/10.1007/s10569-010-9320-4

Bigg, E. K. (1964). Influence of the Satellite Io on Jupiter's Decametric Emission. *Nature*, 203, 1008-1010.

Carr, T. D., Desch, M. D., Alexander, J. K. (1983). Phenomenology of Magnetospheric Radio Emissions. In *Physics of the Jovian Magnetosphere.* 226-284. Cambridge, MA: Cambridge University Press.

Garcia, L. N. (1996). Long Term Periodicities in the Jovian Decametric Emission, (Doctoral dissertation). Gaineville, FL: Univeristy of Florida.

Giorgini, J. D. & JPL Solar System Dynamics Group, NASA/JPL Horizons On-Line Ephemeris System, < http://ssd.jpl.nasa.gov/?horizons >, data retrieved 01 Oct 2020.

Marques, M. S., et al. (2017). Statistical Analysis of 26 yr of Observations of Decametric Radio Emissions from Jupiter. *Astronomy & Astrophysics*, 604, A17-A35. https://doi.org/10.1051/0004-6361/201630025

Seidelmann, P. K. & Divine, N. (1977). Evaluation of Jupiter Longitudes in System III(1965). *Geophysical Research Letters*, 4(2), 65-68.